Interdecadal Variability of the Warm Arctic and Cold Eurasia Pattern and Its North Atlantic Origin

MI-KYUNG SUNG

Ewha Womans University, Seoul, Seoul, South Korea

SEON-HWA KIM AND BAEK-MIN KIM

Korea Polar Research Institute, Incheon, South Korea

YONG-SANG CHOI

*Ewha Womans University, Seoul, Seoul, South Korea, and Jet Propulsion Laboratory,
California Institute of Technology, Pasadena, California*

ABSTRACT

This study investigates the origin of the interdecadal variability in the warm Arctic and cold Eurasia (WACE) pattern, which is defined as the second empirical orthogonal function of surface air temperature (SAT) variability over the Eurasian continent in Northern Hemisphere winter, by analyzing the Twentieth Century Reanalysis dataset. While previous studies highlight recent enhancement of the WACE pattern, ascribing it to anthropogenic warming, the authors found that the WACE pattern has experienced a seemingly periodic interdecadal variation over the twentieth century. This long-term variation in the Eurasian SAT is attributable to the altered coupling between the Siberian high (SH) and intraseasonal Rossby wave emanating from the North Atlantic, as the local wave branch interacts with the SH and consequentially enhances the continental temperature perturbation. It is further identified that these atmospheric circulation changes in Eurasia are largely controlled by the decadal amplitude modulation of the climatological stationary waves over the North Atlantic region. The altered decadal mean condition of stationary wave components brings changes in local baroclinicity and storm track activity over the North Atlantic, which jointly change the intraseasonal Rossby wave generation and propagation characteristics as well. With simple stationary wave model experiments, the authors confirm how the altered mean flow condition in the North Atlantic acts as a source for the growth of the Rossby wave that leads to the change in the downstream WACE pattern.

1. Introduction

Since the continental-scale extreme cold winters that have occurred repeatedly over the Northern Hemisphere in recent decades, many efforts have been made to understand the underlying physical mechanism of cold winters. With a global warming trend, the rapid decrease of Arctic sea ice is blamed as a major cause of the cold winters (Zhang et al. 2012; Tang et al. 2013; Inoue et al. 2012; Honda et al. 2009; Petoukhov and Semenov 2010; Cohen et al. 2012). Observational and numerical evidences have supported the influence of the Arctic sea ice loss on a series of unusually cold winters over Eurasia and North America. Here, Arctic sea ice

influence seems more clearly detectable in the Eurasian continent since the winter weather and climate in North America are equally controlled by remote influences from the tropics as well as from the Arctic (Palmer 2014; Hartmann 2015; Nakanowatari et al. 2015; Watson et al. 2016). As to the Arctic influence on Eurasia, Mori et al. (2014) argued that a climate mode, namely the warm Arctic and cold Eurasia (WACE) pattern, is a direct atmospheric response to the sea ice decline over the Barents and Kara Seas (herein B/K Sea). They showed that the occurrence of subarctic blocking increases with conditions of less sea ice, consequently enhancing continental cold anomalies by exerting cold advection toward the inland areas. For the Eurasian winter climate, it is widely considered that the origin of cold winters over Eurasia is largely attributable to a quasi-stationary

---

Corresponding author: Dr. Baek-Min Kim, bmkim@kopri.re.kr

high pressure anomaly over the B/K Sea, which is established by an anomalous turbulent heat flux from the bare Arctic Sea surface or reduced cyclonic activity due to weaker baroclinicity (Zhang et al. 2012; Tang et al. 2013; Inoue et al. 2012; Honda et al. 2009; Petoukhov and Semenov 2010; Alexander et al. 2004; Ou et al. 2015).

In spite of various evidence supporting the impact of Arctic sea ice loss, counterarguments are also raised (McCusker et al. 2016; Sigmond and Fyfe 2016; Barnes and Screen 2015). McCusker et al. (2016) argued that the observed cooling over central Eurasia was probably due to a sea ice–independent internally generated circulation pattern ensconced over the B/K Sea since the 1980s. It is noteworthy that while Mori et al. (2014) and McCusker et al. (2016) both conducted large ensemble simulations of climate models to depict the forced atmospheric response to sea ice reduction, their conclusions are quite different. The discrepancy between the earlier researches can be due to the large internal variability in the Arctic climate system resulting from complicated physical processes and feedbacks between them to lead to the Arctic warming, in addition to the impacts of the sea ice reduction (Screen et al. 2013, 2014; Barnes and Screen 2015). This means that knowing about underlying processes that contribute to the Arctic warming can be essential to resolve the contradiction.

With regard to this, it is worth noticing the studies addressing the atmospheric energy transport from outside of the Arctic. While the direct impact of reduced sea ice tends to appear in the lowermost part of the atmosphere, the Arctic temperature change is observed above the surface layer as well (Graversen et al. 2008). Recent studies identify a considerable contribution of the heat and moisture transport in the Arctic warming through atmospheric wave response, and it accounts for the observed Arctic thermal structure well (Yang et al. 2010; Woods et al. 2013; Nakanowatari et al. 2014; Sato et al. 2014; Park et al. 2015; Woods and Caballero 2016; Jung et al. 2017). Particularly, the impact of moisture transport from outside of the Arctic is identified to be important, as it accelerates the Arctic surface warming through downward infrared radiation (Park et al. 2015). In spite of increasing evidence suggestive of the crucial role of the atmospheric transport, however, it is still mysterious what controls the atmospheric circulation change.

From historical records on the Arctic sea ice extent, we may find a key for the current warming situation. Some studies revealed a pronounced warming amplified in the Arctic during the midtwentieth century, which is quite analogous to the current warming (Bengtsson et al. 2004; Miles et al. 2014; Tokinaga et al. 2017). These studies suggest that natural variability such as the

Atlantic multidecadal variability can be a likely cause for the earlier warming, whereas the later one is attributable to anthropogenic forcing. Nevertheless, it seems highly uncertain whether the Arctic warming of the late twentieth century is solely being driven by the anthropogenic forcing, since the evidence of atmospheric transport from outside of the Arctic can allude to the incorporation of internal variability in the current Arctic warming. In this study, we attempt to comprehend the dynamical process involved in the Arctic warming as well as concurrent continental cold by investigating how the atmospheric circulation has been modulated in the long-term time scale.

To do this, the past interdecadal variability is assessed by focusing on the WACE pattern, which captures the temperature contrast between the B/K Sea and the Eurasia continent. It is meaningful to investigate this regional characteristic since the Arctic sea ice reduction relevant to moisture intrusion events is most pronounced in the B/K Sea region (Woods and Caballero 2016). As the wintertime variability of the Eurasian SAT is dominated by a seasonal continental anticyclone, namely the Siberian high (SH), atmospheric perturbations that lead to crucial climatic events over Eurasia, such as cold surges, tend to accompany the abnormal growth of the SH (Ding and Krishnamurti 1987; Joung and Hitchman 1982; Takaya and Nakamura 2005a,b). In this study, therefore, we investigate an interaction between the SH and upper-level atmospheric circulation in order to obtain a useful insight on the dynamics behind the meridional temperature contrast of the WACE pattern.

In section 2, we describe the data and model. We investigate the spatiotemporal variability of the WACE pattern in section 3 as well as the underlying dynamical process involved with the SH in section 4. In section 5, an atmospheric background flow condition over the North Atlantic region that modulates the changes described in the previous section is addressed. In our conclusions and discussion, we briefly note the possible role of internal variability in current global warming and the implications for the future climate.

2. Data and methods

We mainly used the National Oceanic and Atmospheric Administration/Cooperative Institute for Research in Environmental Sciences (NOAA/CIRES) Twentieth Century Reanalysis project, version 2c, dataset (20CR) (Compo et al. 2011) with a horizontal $2° \times 2°$ grid and temporal 6-h resolution spanning 1850–2014. The 20CR utilized only surface observations of synoptic pressure for assimilation and observed monthly

SST and sea ice distributions are used as model lower boundary conditions. According to Paek and Huang (2012), 20CR provides reliable estimates of decadal to multidecadal variability of the upper-tropospheric circulation in general. To enhance the reliability of our analysis as much as possible, we compared 20CR with other datasets, such as the National Centers for Environmental Prediction (NCEP)–National Center for Atmospheric Research (NCAR) reanalysis (Kalnay et al. 1996) in the overlapping period, and obtained overall good agreement in blocking frequency and spatiotemporal variability of major climate modes (not shown). With regard to the blocking frequency, however, we found that long-term mean characteristics significantly differ before and after 1900 (data not shown). Therefore, we performed the analysis only after 1901 (i.e., 1901–2014). The 20CR data provide 56 ensemble members for estimating the uncertainty, and we used the mean of all ensemble members of the atmospheric variables in the analysis. The analysis was based on the seasonal mean of boreal winter [December to the following February (DJF)], and an anomaly was simply defined as a departure from the winter mean climatology (DJF average).

Following the methodology by Mori et al. (2014), we defined the WACE pattern by applying an area-weighted empirical orthogonal function (EOF) analysis to SAT anomalies over the Eurasian continent (20°–90°N, 0°–180°) for the period of 1901–2013. The second principal component time series (PC2) is referred to as the WACE index following Mori et al. (2014). During the entire analysis period, the WACE index exhibited noteworthy interdecadal fluctuation. This long-term variation was pronounced especially between the following four periods of 1901–29 (P0), 1930–54 (P1), 1955–79 (P2), and 1980–2013 (P3). We show in section 5 that the distinct characteristics for each period result from intrinsic changes in the upstream atmospheric circulation, which provides the basis for the division of P0–P3. The intensity of the SH was represented by area-averaged sea level pressure (SLP) anomalies over the region of maximum climatological high pressure (40°–60°N, 70°–120°E) as in Gong et al. (2001).

To detect the atmospheric blocking, we adopted a hybrid blocking index proposed by Dunn-Sigouin et al. (2013) for the daily ensemble mean 500-hPa geopotential height (Z500) field. In detail, the hybrid blocking index combines two widely used blocking indices, the Dole–Gordon index (Dole and Gordon 1983) and the Tibaldi–Molteni index (Tibaldi and Molteni 1990). The process for detecting the blocking starts by identifying a contiguous area of blocking anomalies, as in the Dole–Gordon index; then a reversal of the meridional gradient of geopotential height is evaluated in the southward direction of the blocking anomaly maximum, as in the Tibaldi–Molteni index. The blocking frequency is defined as a percentage of blocked days to the number of wintertime days (90 days) per each year. Please refer to Dunn-Sigouin et al. (2013) for a more detailed methodology.

In addition to the observational analysis, we also performed simple model experiments to assure a dynamical process related to the WACE pattern using a stationary wave model (SWM) (Ting and Yu 1998). The SWM is a nonlinear baroclinic model with a dry dynamical core and 14 vertical levels on sigma coordinates. Its horizontal resolution is truncated at rhomboidal 30, and experiments were designed to have idealized forcing with a sine-squared function form corresponding to vorticity flux convergence by transient eddies. The detailed calculation of the forcing is given as

$$\text{TF}_{\text{vor}} = -\nabla \cdot (\overline{\mathbf{V}'\xi'}),$$

where ξ is the vorticity and $\mathbf{V}$ is the horizontal wind. The bar represents the seasonal mean for DJF and the prime shows daily anomalies, which are applied by a 2–8-day bandpass filter. The response to the forcing shown here is averaged for 50 days, since the steady forcing is exerted. Further details of the model equations or information can be found in Ting and Yu (1998) and Wang and Ting (1999).

3. Long-term spatiotemporal variability in the Eurasian surface air temperature

The wintertime SAT fluctuation over Eurasia is known to be strongly coupled to the Arctic Oscillation (AO), which dominates the atmospheric circulation over the Northern Hemisphere (Thompson and Wallace 1998). As noticed in Mori et al. (2014), this relation is reflected in the first EOF (EOF1) of the Eurasian SAT, which is characterized by uniform warming over the entire Eurasian continent (Fig. 1a). A high correlation coefficient between the first principal component time series (PC1) of the Eurasian SAT and the AO index ($r = 0.7$) supports the intimate relation. On the other hand, the second leading mode (EOF2) of the Eurasian SAT shows clear dipolar temperature anomalies straddling over the B/K Sea and inland Eurasia (Fig. 1b). Mori et al. (2014) referred to this meridional temperature contrast as the WACE pattern and highlighted that the WACE pattern was recently amplified due to the sea ice decline over the B/K Sea. It is noteworthy that we obtained almost identical patterns in the first two leading modes even though the analysis period of this study covers the entire twentieth century whereas the earlier study utilizes the data only for about the last
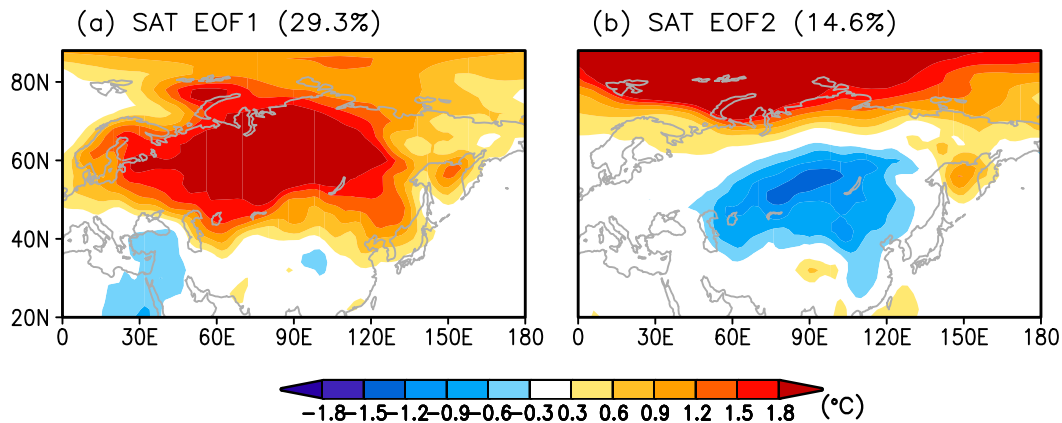
FIG. 1. (a) The first and (b) second principal components of the SAT anomalies over Eurasia (20°–90°N, 0°–180°) during winters of the 1901/02–2013/14 DJF. The second pattern is defined as the WACE pattern following Mori et al. (2014).

three decades. In particular, the pronounced temperature dipole pattern for the entire twentieth century may imply that the WACE pattern is a part of internal mode of the Eurasian SAT variability.

To check the robustness of the WACE pattern during the past century, we examined the spatiotemporal variability of the Eurasian SAT by applying the EOF analysis separately for the four subperiods (i.e., P0–P3). As shown in Fig. 2, each EOF2 for P0–P3 shows the distinct spatial distribution of the SAT anomalies. Specifically, the anomalies for P0 display quite distinct features from the WACE pattern (Fig. 1b), which is defined as the EOF2 for the entire analysis period in this study. The warm anomaly is relocated over northern Europe, while the center of the continental cold anomaly is found near the Caspian Sea. Overall, the distribution of anomalies for P0 seems to be shifted westward compared to that of the WACE pattern shown in Fig. 1b. By contrast, the EOF2 for P1 (Fig. 2b) seems similar to the WACE pattern which has warm and cold counterparts positioned over the B/K Sea and central Siberia (black squared region), respectively.

The distinct difference between P0 and P1 may be due to less reliable data during the former period, since the number of observation stations incorporated in 20CR data is much sparser during P0 than the latter period. However, the shifted pattern in P0 may not be solely an error due to the weak data confidence. The SAT anomalies during P2 are also notably shifted to the west as in P0. Although an extra warming signal is found over the B/K Sea region during P2 (unlike P0), the overall distributions of temperature anomalies for P0 and P2 closely resemble each other. In fact, for P0, the meridional temperature contrast between the B/K Sea and inland Eurasia is more pronounced in EOF3 than in EOF2, although the spatial structure of the anomalies in EOF3 is not the same as the typical WACE pattern (Fig. 2e). It seems that EOF2 and EOF3 for P0 are not separated completely, as can be inferred from the slight difference between their loading percentages (13.5% for EOF2 and 11.3% for EOF3) (North et al. 1982). Nevertheless, what we can identify from the characteristics in these two orthogonal functions is that dominance of the typical WACE pattern was reduced while westward shift tendency of the anomalies became robust during P0 likewise P2. Thereafter, the EOF2 for P3 again shows the prominent dipolar pattern between B/K Sea and central Siberia (Fig. 2d). Conspicuously, the spatial characteristics of the anomalies between P1 and P3 are almost identical, and the loading percentages are also comparable between the two periods (18.2% for P1 and 18.5% for P3).

Although the EOF results for the four subperiods show distinct characteristics by decades, they seem to reflect inherent characteristics of the WACE pattern as inferred by the correlation analysis in Table 1. We can find that the correlation between the WACE index and PC2 for P2 reaches 0.86, which is highly comparable to those of P1 and P3, even though the spatial characteristics of the EOF2 for P2 are distinguishable from those of P1 and P3 periods as aforementioned. The high correlation between the PC2 and the WACE index for P2 period may suggest that the westward shifted temperature distribution reflects a long-term internal variability in the Eurasian SAT, and likewise for P1 and P3. On the other hand, the correlation for P0 is very low between the WACE index and the PC2 ($r = 0.13$). Nevertheless, we should take EOF3 into account together with EOF2 (the correlation between PC3 and WACE index is 0.82), and we can infer from the two inseparable modes that
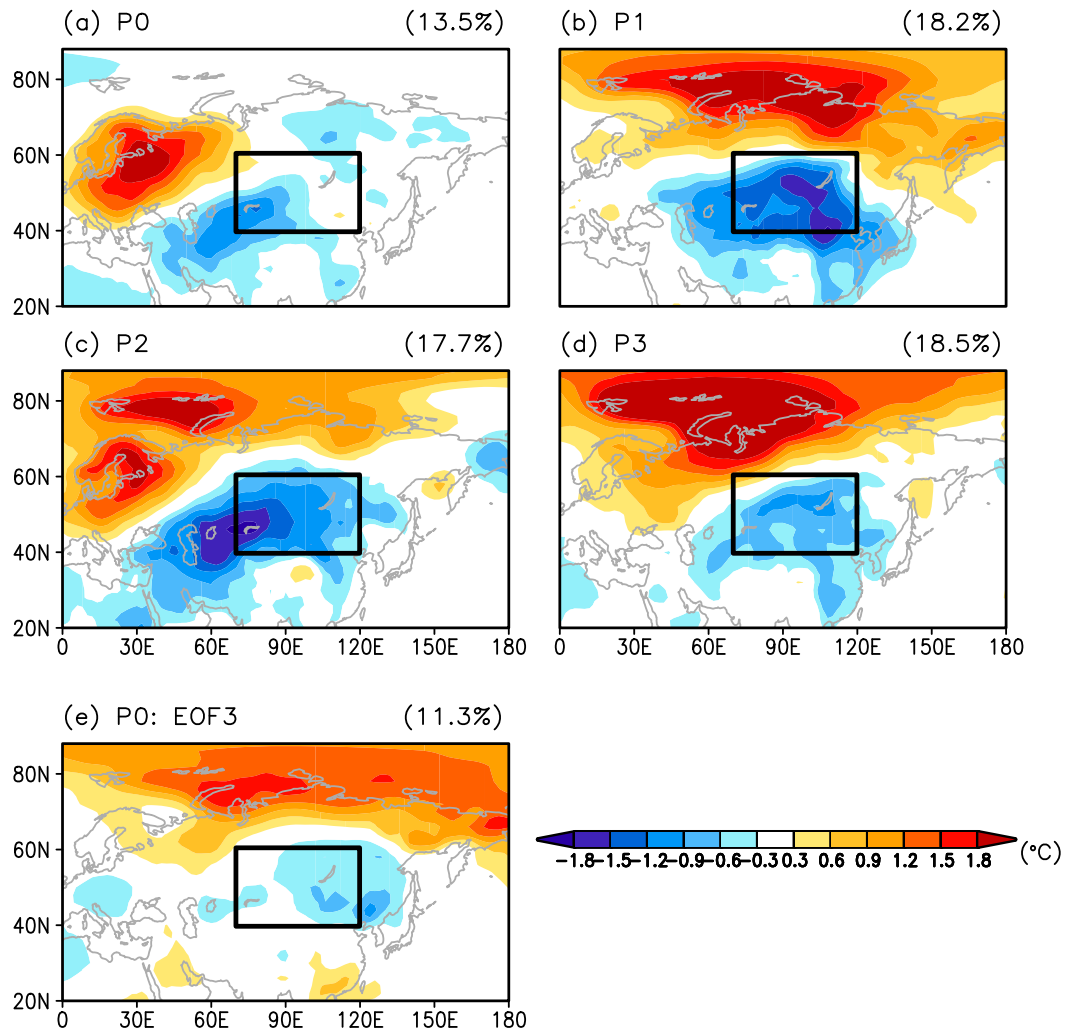
FIG. 2. The second EOF patterns of SAT over the Eurasia domain (20°–90°N, 0°–180°) during the (a) P0, (b) P1, (c) P2, and (d) P3 subperiods, respectively. (e) The third EOF pattern of SAT during PO. Rectangle denotes the domain of the SH index definition.

the spatial variability of the SAT during P0 is not likely the same as the typical features of the WACE pattern.

The spatial distributions of the temperature anomalies between the EOF2s for P0 and P2 and for P1 and P3 seem to depict a periodic variation at an interdecadal time scale. This long-term variation has an important implication from a regional climate change perspective. The pronounced temperature contrast between the Arctic and Eurasia during the P3 period is often attributed to the Arctic warming due to the sea ice loss and consequent cooling over the inland region (Mori et al. 2014; Tang et al. 2013; Inoue et al. 2012). On the other hand, a reason for the noticeable dipolar temperature variability during P1 can be inferred from some observational studies dealing with historical records in the Arctic during the entire twentieth century

(Johannessen et al. 2004; Bengtsson et al. 2004; Miles et al. 2014). These studies report that Arctic sea ice had decreased pronouncedly during 1930s to 1940s, indicating an apparent warming tendency of the Arctic during this period. This implies that the noticeable dipolar temperature variability during P1 is likely corresponding to the mid-twentieth-century Arctic warming. Furthermore, the similarity between P1 and P3 possibly implies a dynamical mechanism to modulate the long-term internal variability in the Eurasian SAT. To understand this spatiotemporal variability in the Eurasian SAT, in section 4 we investigate the dynamical processes by which the meridional temperature contrast is enhanced.

Unlike the distinct interdecadal variation in EOF2 of the Eurasian SAT, we did not find any noteworthy

TABLE 1. Correlation coefficients between the PC1 of Eurasian SAT for entire period (1901–2013) and those for P0–P3 (subperiods), as well as the correlation coefficient between the WACE index and PC2 for P0–P3.

Correlation between leading EOFs of Eurasian SAT	P0 (1901–29)	P1 (1930–54)	P2 (1955–79)	P3 (1980–2013)
PC1 (entire period) vs PC1 (subperiod)	0.98	0.99	0.98	0.94
PC2 (entire period) (=WACE index) vs PC2 (subperiod)	0.13	0.88	0.86	0.80
WACE index vs PC3 (subperiod)	0.82			

difference between each EOF1 for P0–P3 and that for the entire period (Fig. 3). The EOF1 patterns for the four subperiods show continent-wide warming dominating across northern Europe and Siberia, similar to the results for the entire twentieth century, although the local magnitudes of anomalies slightly differ by region. Table 1 shows that each PC1 for P0–P3 coincides quite well with the PC1 for the entire period. This stationary feature in EOF1 implies that the continent-wide warming or cooling is a leading characteristic in the Eurasian SAT variability irrespective of decades.

4. Atmospheric circulation to enhance the warm Arctic and cold Eurasia pattern and intermediate role of the SH

To understand the long-term variation related to the WACE pattern in more detail, first we examined the relevant atmospheric circulation characteristics, especially corresponding to the positive and negative phases of the WACE pattern. Because the Arctic warming that accompanies the cold continent situation is often highlighted as an issue of the recent decade, we need to check opposite characteristics of the WACE pattern to understand the variations for other decades. Figure 4 shows composite anomalies for positive and negative phase years of the WACE index. In Fig. 4b, a typical WACE pattern is identified and, in contrast, a roughly opposite "cold Arctic and warm Eurasia" pattern is found in Fig. 4c. Although the anomalous features between the two composite analyses are roughly symmetric, the details are rather different. While the continental cold anomaly during positive WACE (+WACE) years tends to be confined to the region of climatological stationary anticyclone (see Fig. 4a for SLP climatology), during negative WACE (−WACE) years, the Eurasian warm anomaly becomes zonally
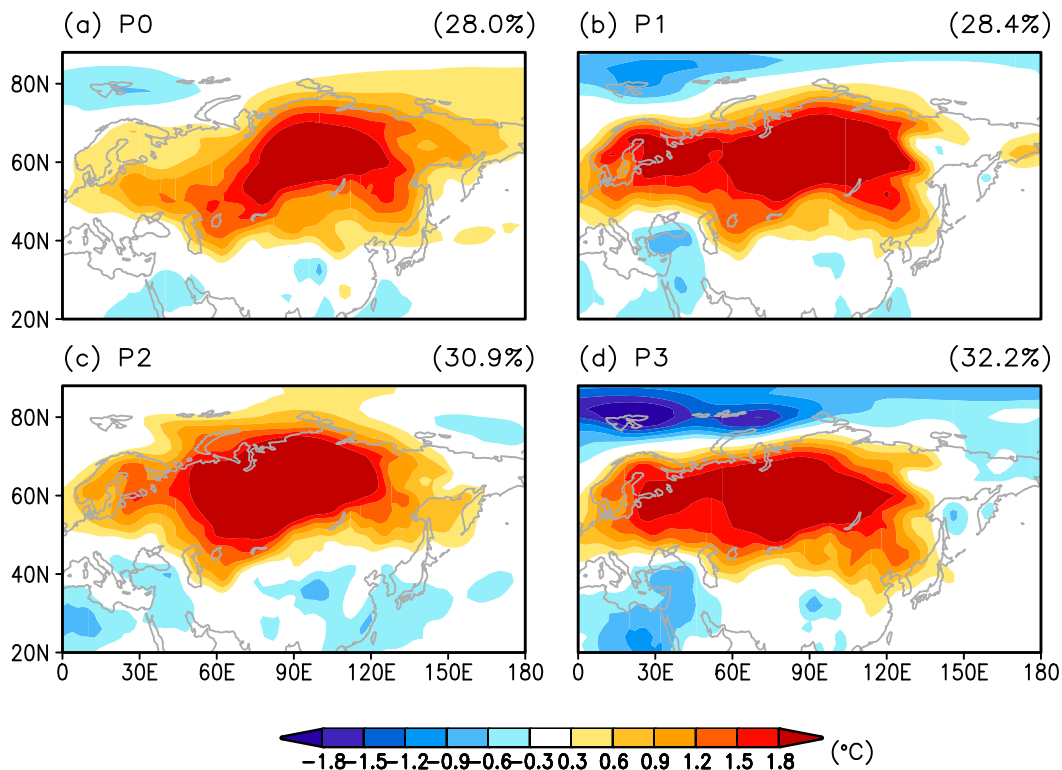

FIG. 3. The first EOF patterns of SAT over the Eurasia domain (20°–90°N, 0°–180°) during the (a) P0, (b) P1, (c) P2, and (d) P3 subperiods, respectively.
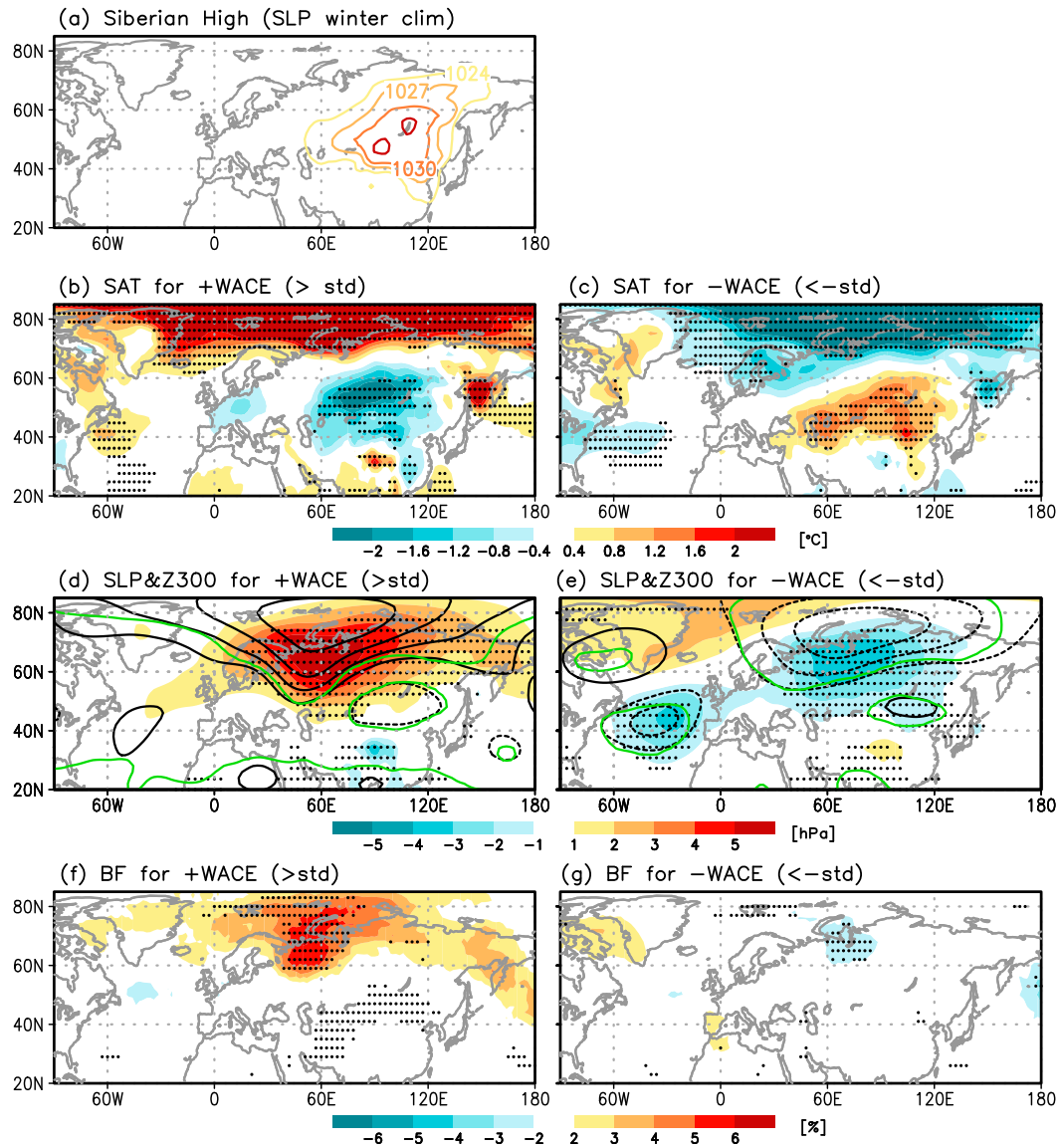
FIG. 4. (a) Climatological mean of the SLP exhibiting the Siberian high (isobars above 1024 hPa are denoted only). (b) Composite anomalies of SAT for positive WACE years (>1 std dev, 14 yr) and (c) those for negative WACE years (<−1 std dev, 19 yr). (d),(e) As in (b),(c), but for the SLP (shading) and Z300 (contour) anomalies, respectively. Contour interval is 20 m. (f),(g) Anomalous blocking frequency for +WACE and WACE years. Stippling indicates regions exceeding 95% confidence level on a *t* test for shaded anomalies.

elongated and extends far westward. Furthermore, in the Arctic region, the cold anomaly during −WACE years also extends more into the Scandinavian peninsula. This contrasts with +WACE years, whose warm anomaly is excluded from the land and confined only over the Arctic Ocean. Besides these spatial differences, the magnitude of the continental anomaly tends to weaken during −WACE years.

We can relate these phase-dependent characteristics in the SAT anomalies to the local circulation over the B/K Sea region. In Fig. 4d, the SLP anomalies

corresponding to +WACE years shows a strong surface anticyclone that seems to span from the Ural Mountains across Siberia (shading) while the upper-tropospheric ridge, which is bulging to the south, is centered over the B/K Sea region (contour). These seasonal averaged features in the atmospheric circulation seem to result from an increased occurrence of blocking over the B/K Sea region at an intraseasonal time scale as shown in Fig. 4f. The increased blocking occurrence is known as a representative characteristic that is often accompanied by Arctic surface warming over the B/K Sea, although
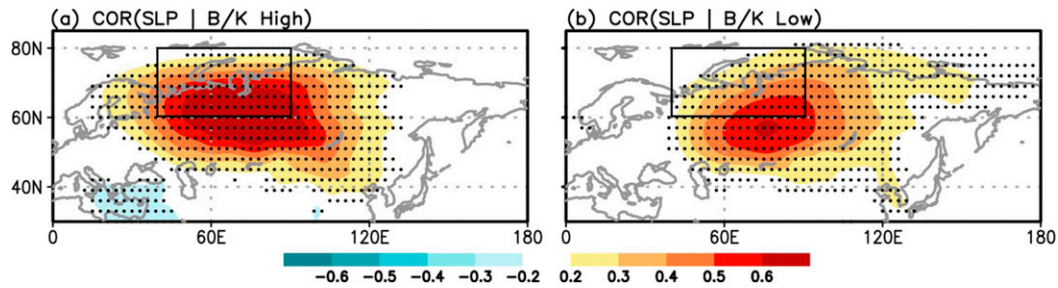
FIG. 5. Correlations of monthly SLP anomalies with upper-tropospheric circulation (Z300) intensity over the B/K Sea (60°–80°N, 40°–90°E; region marked by a rectangle) during winter (DJF). Correlations were calculated conditionally when the Z300 anomaly over the B/K Sea is (a) positive and (b) negative. Stippling indicates regions exceeding 95% confidence level on a t test.

the relevant dynamics is not yet established (Luo et al. 2016; Mori et al. 2014). On the other hand, the large-scale circulation anomalies for −WACE years show almost opposite features over Eurasia from those of positive years (Fig. 4e). We can find an upper-level trough, which is more zonally oriented along the B/K Sea coastline, as well as a decreased blocking frequency at the same region (Fig. 4g).

The circulation anomalies during +WACE years over Eurasia resemble a typical pattern promoting the SH intensification (Sung et al. 2011; Takaya and Nakamura 2005a; Joung and Hitchman 1982). Since the variability of the Eurasian temperature is largely determined by the interaction between climatological surface anticyclone and the upstream perturbation, it is important to examine how the SH responds to the altered circulation during ±WACE years in order to understand the altered SAT distributions. With regard to this, Sung et al. (2010) described an asymmetric growth of the SH in association with the opposite-signed upstream flow anomalies, and we can find consistent relations in Fig. 5. An anticyclonic circulation over the B/K Sea exhibits strong correlation with the SLP in inland Eurasia, which implies strong growth of the SH when the upstream circulation over the B/K Sea region has the same-signed vorticity characteristic with the SH. On the contrary, a weaker correlation of the SLP in Fig. 5b can indicate relatively weaker attenuation of the SH when the upstream circulation is cyclonic.

The reason for these asymmetric responses of the SH is not clear, but a dynamical process promoting the growth of the SH may give a hint. According to Takaya and Nakamura (2005a), on an intraseasonal time scale a blocking high over upstream subarctic region reinforces the SH by inducing an anomalous cold advection. The intensified surface high, in turn, acts to induce anomalous vorticity advection aloft that strengthens the upstream ridge, which facilitates the growth of the SH by further enhancing cold advection. This vertical coupling

process can work in both ways to amplify or attenuate the SH in accordance with the upstream circulation characteristics. However, the phase-asymmetric correlations in Fig. 5 suggest that the coupling strength between upper-tropospheric circulation over the B/K Sea and climatological surface high is not always the same, which is supposedly due to different contributions of mean circulation component of the SH and nonlinear interaction. A qualitative analysis is required for more concrete dynamical understanding, but this is beyond the scope of our study.

The fact that the atmospheric circulation anomalies corresponding to −WACE years do not necessarily bring the linear strong suppression of the SH means that the temperature anomalies over Eurasia corresponding to ±WACE years can be inherently different. Thus, the weak and zonally extended warm continental anomaly during −WACE years could result from the weaker vertical coupling between the subarctic circulation and the SH. Here, it is worth noticing that the time scale of the aforementioned intensification mechanism of the SH is intraseasonal. Therefore, our analysis results suggest that the emergence of the WACE pattern, which is seasonal, can be due to the altered occurrences of subarctic blocking near the B/K Sea and subsequent anomalous intraseasonal development of the SH in winter.

Based on this understanding about the inherent characteristics of the WACE pattern, we investigate the long-term variation of the WACE pattern within P0–P3 addressed in the previous section. Figure 6 shows the relation between the WACE pattern and the SH and its temporal evolution. The black line, which represents the seasonal mean SH intensity, tends to coincide well with the variation of the WACE index denoted by the gray line. For the entire analysis period, the correlation coefficient between the SH and WACE indices reaches 0.53, supporting a crucial importance of the SH in the manifestation of the WACE pattern. Nevertheless, the
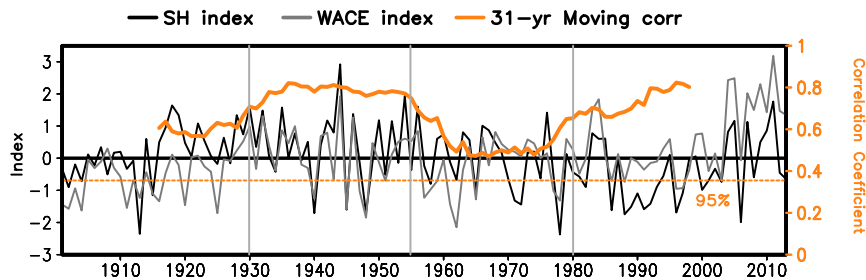
F<small>IG</small>. 6. Normalized Siberian high (SH) index (black line) and WACE index (gray line) during winter of 1901–2013 from 20CR data. The thick orange line represents the 31-yr moving correlation coefficient between the SH and WACE indices (right axis label) and the thin orange dotted line denotes the 95% confidence level on a *t* test.

relationship is not stationary but fluctuates repeatedly between 0.5 and 0.8 as depicted by the orange line. It is clearly seen that the correlation coefficients for P1 and P3 periods are maintained at high values (see the gray vertical segments denoting the period for P0–P3). In contrast, a weaker correlation appears during P0 and P2. This long-term variation of the correlation is possibly associated with the interdecadal phase shift of the WACE index. Note that the temporal variation of the WACE index shows a prominent negative tendency during the P0 and P2 periods: the sign of the WACE index maintained a negative phase during P0 and had less strongly positive peaks during P2. As the atmospheric circulation anomalies associated with –WACE index act to weaken the relation to the SH, the correlation between the WACE and SH indices can become lower during P0 and P2.

The lower correlation can be interpreted that the coupling between the temperature fluctuations in the Arctic and Eurasia becomes weaker during P0 and P2. Likewise, the higher correlation during the P1 and P3 periods indicates stronger coupling between the circulations over the Arctic and Eurasia so that the meridional temperature contrast becomes enhanced as well as the WACE pattern. This enables us to infer that the frequent occurrence of the atmospheric circulation that favors either the positive or negative WACE pattern also affect the horizontal structure of the Eurasian SAT variability, and this is supposedly manifested as the altered EOF2 patterns for P0–P3. Accordingly, it is perceived that the spatiotemporal variation of the WACE pattern can be represented well by the long-term variation of the moving correlation between the SH and WACE indices. On the other hand, the WACE index itself is constrained to represent the spatial variation of the WACE pattern because of spatial stationarity assumption in the EOF analysis.

To further find why and how such a long-term temperature variation appears in the Eurasian continent, we closely look at the upstream differences in the North Atlantic during ±WACE years. Focusing on the North Atlantic, the most conspicuous features in the SAT are an anomalous warming and cooling over the oceanic front region near the Gulf Stream (Figs. 4b,c). It is notable that significant warming and cooling appear in the far upstream oceanic front region relevant to the ±WACE pattern alternately. A possible implication of these temperature anomalies can be found from the earlier studies that examined the impacts of the extratropical ocean on the overlying atmosphere. According to Minobe et al. (2008), changes of the Gulf Stream can affect the remote regional climate by forcing planetary waves. This argument has been supported by studies that highlight the role of the sea surface temperature (SST) gradient (Sampe et al. 2010; Frankignoul et al. 2011; Graff and LaCasce 2012).

Based on these earlier findings, we can conjecture that the temperature anomalies over the North Atlantic would be related to the atmospheric wave that affects the downstream climate. Here it is especially worth noting recent studies that elucidated the trigger mechanism of quasi-stationary planetary waves over the North Atlantic front region (Jung et al. 2017; Sato et al. 2014; Nakanowatari et al. 2014). Jung et al. (2017) revealed that the altered oceanic front conditions due to the anomalous SST can modulate the transient eddies so that the corresponding anomalous vorticity flux acts as a Rossby wave source. They further argued that this planetary wave propagates downstream and enhances the Arctic warming over the B/K Sea region by exerting warm advection. Although the target season analyzed in the previous study is slightly different from ours, the temperature perturbations shown in Fig. 4 possibly allude to the similar dynamical linkage through the Rossby wave response. In the upper troposphere, we can find anomalous features that are consistent with the earlier study. Especially in the −WACE composite (Fig. 4e), meridional dipolar circulation anomalies that
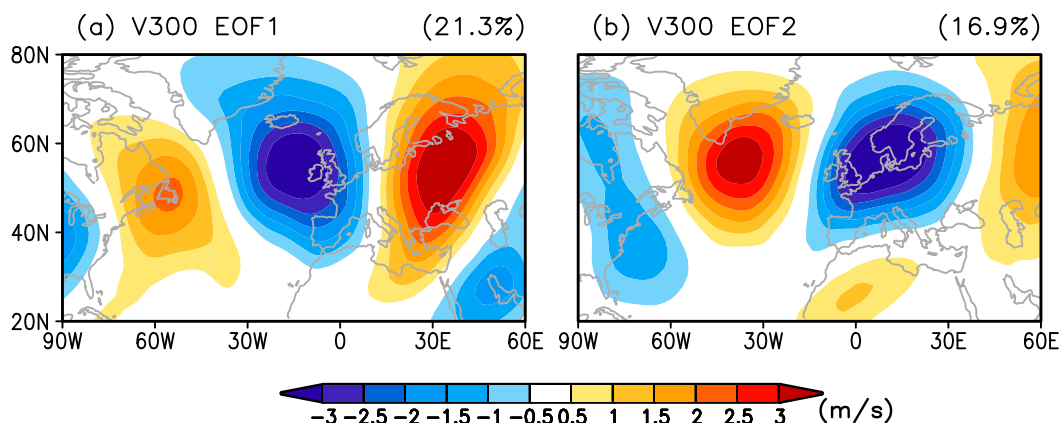
FIG. 7. (a) The first and (b) second EOF mode of wintertime 300-hPa meridional wind (V300) for Atlantic domain (20°–80°N, 90°W–60°E). The second EOF of V300 is referred as the EV2 mode in this study.

have an overall barotropic structure are pronounced over the North Atlantic. Unlike −WACE years, the circulation anomalies for +WACE years seem to have a single cell structure that is anticyclonic (Fig. 4d). But this signal is hardly significant. In section 5, we will show why these different circulation features appear corresponding to the ±WACE pattern. We also demonstrate the underlying process by which the generation of Rossby wave and the downstream climate are modulated in the interdecadal time scale.

5. Internal atmospheric mode leading to interdecadal changes in the North Atlantic and Eurasia

We first examined the background upper-level wind field in the North Atlantic, which is important for determining the propagation of planetary waves, as well as the Rossby wave source (Karoly and Hoskins 1982; Sardeshmukh and Hoskins 1988). Among a wide variety of modes that comprise the variability of the wind field, we found an intriguing coincidence between an oscillatory variation of the meridional wind and the long-term variability of the WACE pattern. Figure 7 depicts the first two leading EOF modes in the meridional wind at 300 hPa (V300) over the North Atlantic domain for the entire data period. While the EOF1 pattern of V300 is characterized by a pronounced northerly to the west of the United Kingdom, the detailed horizontal structure of EOF2 shows an enhanced southerly wind to the south of Greenland. In this study, our focus is on EOF2 of V300, since the atmospheric variability relevant to EOF2 has a noteworthy relation with the downstream climate at an interdecadal time scale as shown in Fig. 8. We refer to this mode as the EV2 mode hereafter. Shading in Fig. 8 presents the inherent temporal variation of the EV2 mode. For a better recognition of the long-term

variation, we applied a 31-yr moving average to the EV2 index (i.e., the principal component time series of the EV2 mode). The slow ups and downs in the long-term mean EV2 index coincide surprisingly well with the temporal variation of the correlation coefficients between the SH and WACE indices (orange line). We utilized the correlation time series in order to represent the long-term variability of the WACE pattern, since it reflects the spatiotemporal variation of the WACE pattern rather than the WACE index as aforementioned. We emphasize that these coincidences are not accidental, but rather due to changes in the background flow characteristic to generate the quasi-stationary Rossby wave.

To understand the detailed dynamics, we need to see relevant changes accompanied with the EV2 mode. The atmospheric circulation corresponding to the EV2 mode can be recognized readily from the relevant Z300 anomalies (see Fig. 9a, denoted by shading). An anticyclonic anomaly is conspicuous in the middle of the North Atlantic domain. To the northwest, it is accompanied by an anomalous trough centered over the Davis Strait region. This distinct anomalous ridge and trough are positioned in phase with the climatological ridge and trough (contour), respectively. Accordingly, the anomalous Z300 pattern in Fig. 9a can be interpreted to indicate a deepened climatological wave structure condition. This implies that the EV2 mode captures the intensity variation of the climatological stationary wave system over the North Atlantic.

A potential influence of the long-term variation in the EV2 mode can be supposed from the anomalies in atmospheric baroclinicity. Although a precise measure for the atmospheric baroclinicity should be assessed from vertical wind shear, an approximate change can be noticed from the upper-tropospheric zonal wind anomaly (Fig. 9b), which projects the regression coefficient onto
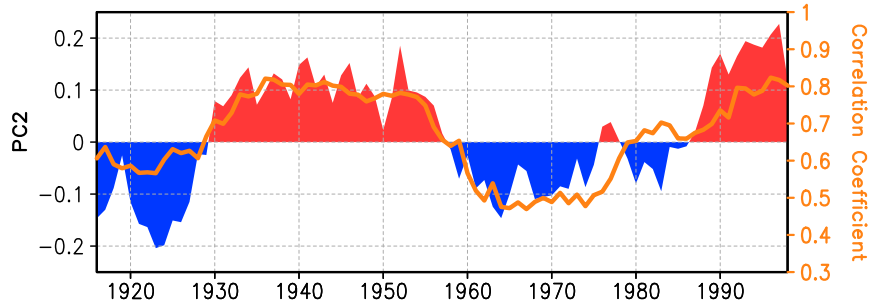
FIG. 8. 31-yr moving average of the EV2 index (shading). The orange line depicts 31-yr moving correlation coefficients between the SH and WACE indices, as shown in Fig. 6.

the EV2 index. The westerly wind strengthens over the northeastern edge of the climatological jet stream due to the intensified pressure gradient relevant to the deepened ridge there. In contrast, the westerly wind weakens to the southeastern boundary of the jet. The change in the baroclinicity is of crucial importance for the behaviors of atmospheric transient eddies and is accompanied by a systematic change in the variance field of transient eddies (i.e., the change in storm track), as recognized in Fig. 9c. We especially pay attention to the altered congregative behavior of the transient eddies, since the vorticity flux convergence due to the anomalous transient eddy flow (TF$_{vor}$) can act as a source to trigger the quasi-stationary atmospheric Rossby wave train (Jung et al. 2017; Sung et al. 2016; Lim 2015). As expected, we can find consequent anomalies in the transient eddy vorticity flux (Fig. 9d). The transient eddy vorticity flux anomalously converges along the southeastern coastal region of Greenland, whereas it diverges over the regions farther south. Both convergence and divergence of vorticity flux can be understood as a necessary response followed by the enhanced EV2 mode.
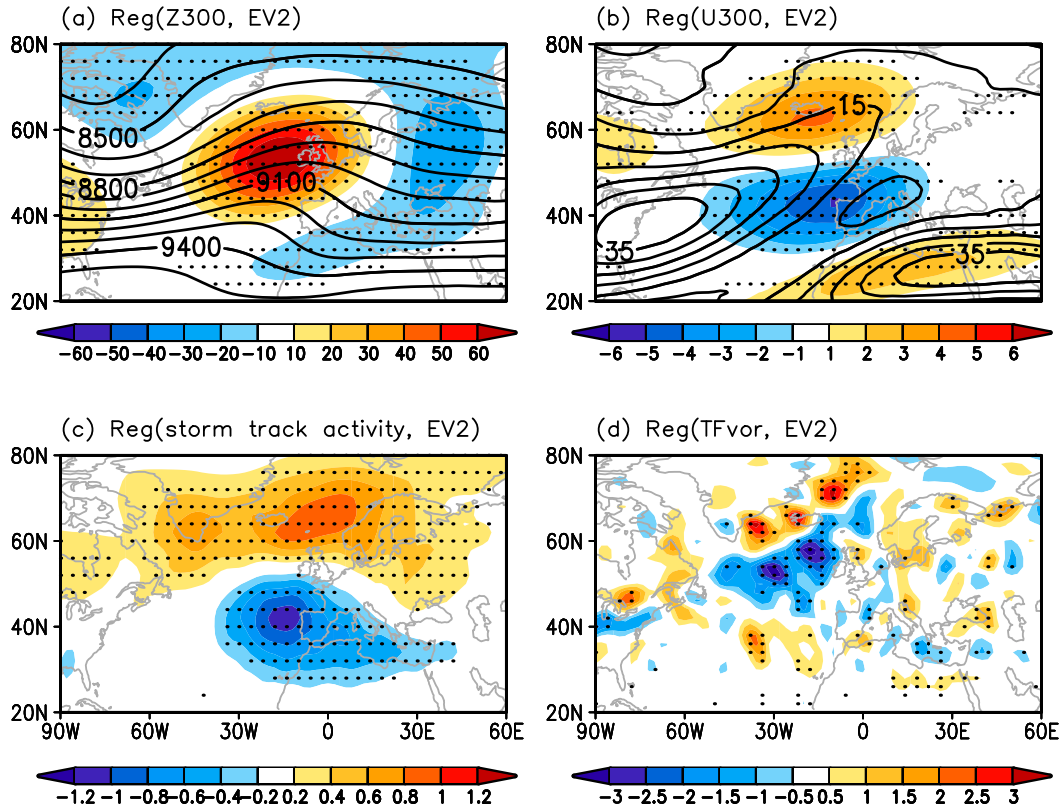

FIG. 9. Regressed anomalies (shading) of (a) Z300, (b) 300-hPa zonal wind (U300), (c) variance of 2–8-day bandpass filtered V300, and (d) transient eddy vorticity flux convergence (interval is $0.5 \times 10^{-11}\,\mathrm{s}^{-2}$) onto the EV2 index. Stippling indicates regions exceeding 95% confidence level on a t test. Contours in (a) and (b) display climatological Z300 and U300.
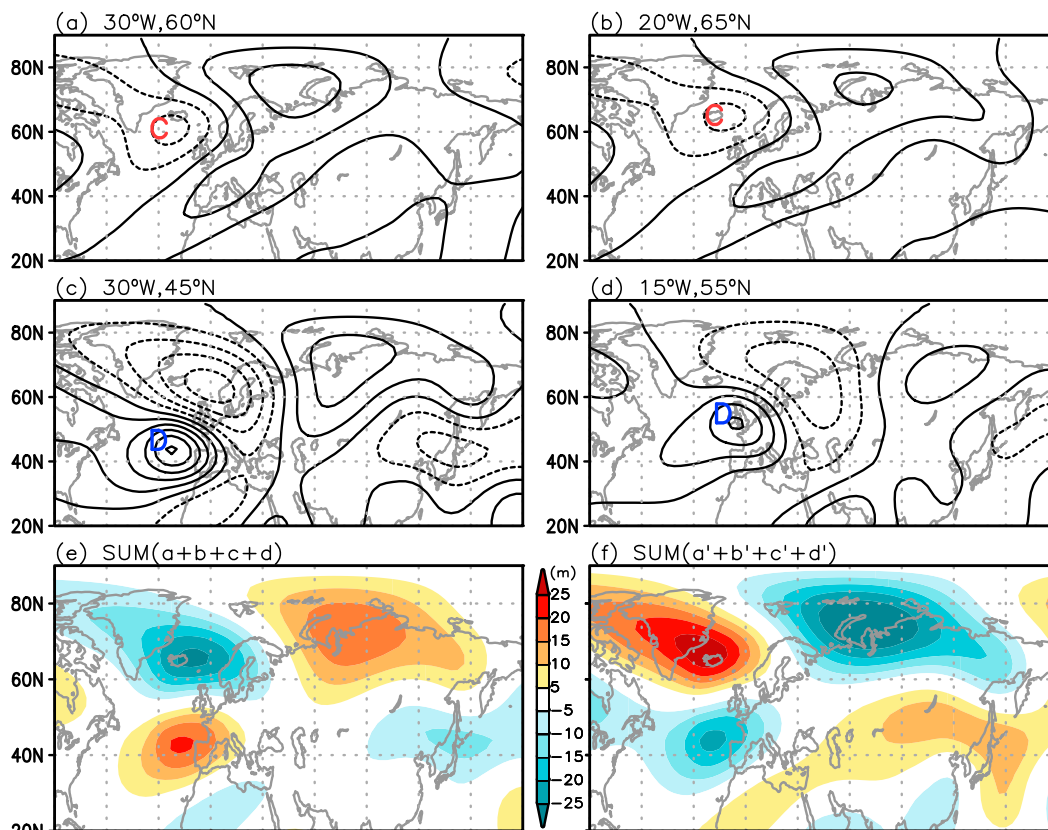
FIG. 10. SWM response of geopotential height at 300 hPa to the pointwise transient eddy vorticity flux convergence forcing located over (a) 60°N, 30°W and (b) 65°N, 20°W (denoted by red capital letter C) and divergence forcing over (c) 45°N, 30°W and (d) 55°N, 15°W (denoted by blue capital letter D) under background flow condition corresponding to +EV2 mode. (e) Linear combination of the responses in (a)–(d). (f) As in (e), but for the background flow condition corresponding to the −EV2 mode and consequent pointwise vorticity flux forcing. Model streamfunction response was converted to geopotential height by being divided by gravity constant 10^{-5} and presented at a contour interval of 3 m.

A possible impact of the anomalous vorticity flux convergence by the change in the congregative storm track condition can be assessed by the SWM, which directly shows the atmospheric response to the anomalous vorticity forcing. We designed a SWM experiment forced by an idealized pointwise TF_{vor}, which is located at a point with markedly strong transient eddy vorticity flux convergence or divergence in Fig. 9d. The background state for the SWM experiments was prepared by adding one standard deviation perturbation corresponding to the +EV2 mode to the full three-dimensional climatological flow during DJF so as to make the background flow consistent to the given forcing. Figures 10a–d show the geopotential height responses to each pointwise convergence forcing given at 60°N, 30°W and 65°N, 20°W as denoted by a red capital letter C and divergence forcing at 45°N, 30°W and 55°N, 15°W as denoted by a blue capital letter D, respectively. In Figs. 10a and 10b, a cyclonic perturbation grows from the forced region near Iceland

and propagates downstream, while a prominent anticyclonic circulation appears over the middle of the North Atlantic when vorticity flux divergence forcing is exerted (Figs. 10c,d). It is notable that the atmospheric responses overall bring an anticyclonic circulation over the B/K Sea region that is crucial for the growth of the WACE pattern as described in the previous section. If we combine all the responses to the four pointwise forcing, we can obtain more realistic wave response to the forcing associated with +EV2 mode (Fig. 10e). Actually, this wave train pattern seems similar to the Z300 anomalies in Fig. 4d, although the cyclonic branch near Iceland is not clear in the +WACE composite.

Then, in order to examine the Rossby wave response to the opposite phase of the EV2 mode (i.e., −EV2 mode), we performed another set of SWM experiments with opposite-signed pointwise forcing. Considering the altered waveguide influence, we prepared the background flow condition by subtracting one standard

deviation perturbation corresponding to the EV2 mode from the climatological mean flow. Figure 10f presents the result in which all the responses to pointwise forcing were combined likewise in Fig. 10e. We can find overall similar but opposite-signed features to those of +EV2 experiment. Consistently, the detailed shape of the wave response closely resembles the observation shown in Fig. 4e. Note that the atmospheric circulation anomalies corresponding to the –WACE pattern are characterized by a meridional dipole structure over the North Atlantic and a zonally oriented cyclonic branch over the B/K Sea region. These are well identified in the simulated results in Fig. 10f. It is notable that the simulated wave characteristics are quite comparable to those of observed ±WACE pattern, even though we applied highly simplified forcing in the simple model. The overall similarity supports a possible impact of the background flow condition corresponding to the EV2 mode on the development of the WACE pattern through the Rossby wave bridge. The smaller wave amplitude of the simulation than the observation in Fig. 4 seems to be an inherent difference between waves corresponding to the EV2 and the WACE pattern, but the absence of coupling process with the SH in the SWM simulation might affect the difference.

Although the model responses indicate a quasi-stationary Rossby wave feature, it does not mean that the anomalous TF_{vor}, related to the long-term phase transition of the EV2 mode, induces a notable stationary wave branch over the downstream B/K Sea whose amplitude is equivalent to that of Fig. 10. This is because the order of the TF_{vor} anomaly corresponding to the interdecadally varying component of the EV2 index is much smaller than the TF_{vor} forcing exerted in the SWM experiments. Therefore, the following direct wave response itself would be feeble. Rather, such a small change in the anomalous vorticity forcing varying in interdecadal time scale is expected to serve as a constraint for a frequently growing quasi-stationary Rossby wave response. In other words, it is likely that the anomalous vorticity flux convergence and divergence during the positive decades of long-term mean EV2 mode, such as P1 and P3, act to increase the probability of the particular shape of the Rossby wave, which is close to that in Fig. 10e. The frequent development of this Rossby wave accordingly leads to the frequent occurrence of the anticyclonic anomaly over the B/K Sea region. The strong cold anomaly over Eurasia during P1 and P3 thus can be regarded as due to the frequent strong interaction between the anticyclonic Rossby wave branch and the SH under the positive EV2 mode–like background flow, which provides a favorable condition for the growth of the Rossby wave. In contrast,

during the negative decades corresponding to the long-term mean EV2 mode, such as P0 and P2, the sign of the vorticity flux forcing would become reversed from that of Fig. 9d. Then, the Rossby wave frequently grows in the shape of Fig. 10f and accompanies a cyclonic branch over the B/K Sea region. Therefore, the −WACE pattern is likely to develop during negative EV2 decades as in P0 and P2.

We can find some more evidence to support the relationship between the quasi-stationary Rossby wave growth and the EV2 mode. Figure 11 shows atmospheric circulation characteristics for the P0–P3 periods corresponding to the WACE index. In Figs. 11a–d, the upper-level circulation anomalies (contours) over the Eurasia region are seemingly analogous, wherein an anomalous anticyclone is pronounced over the B/K Sea. As aforementioned, this upper-level anticyclone is the representative characteristic of the atmospheric circulation that acts to enhance the +WACE pattern. On the contrary, the upstream circulations show distinct differences between the periods. The anomalies for P0 exhibit an anticyclonic circulation over the North Atlantic that accompanies a cyclonic counterpart to the north, although the northern circulation does not seem significant enough. Meanwhile, P1 shows hardly significant perturbations, namely a faint anticyclonic anomaly in the middle of the North Atlantic. These circulation characteristics in P0 and P1 appear coherently for P2 and P3 as well: whereas the meridional dipolar circulation anomalies are found straddling over the North Atlantic during P2, only an insignificant single anticyclonic perturbation is found for P3.

The circulation features for P0 and P2 seem highly consistent with the wave response in the SWM. Especially, the dipolar wave structure over the North Atlantic and zonally elongated wave branch over the B/K Sea are quite similar to Fig. 10f, which shows the favorable wave structure under the background flow condition of the negative EV2 mode. Note that the signs of anomalies in Fig. 10f should be reversed for the right comparison with Fig. 11, since the regression coefficient in Fig. 11 presents the perturbations corresponding to the unit increase of the WACE index while Fig. 10f shows the circulation pattern corresponding to the negative WACE pattern. Recall that the WACE index during P0 and P2 tends to be negative as mentioned in section 4. We can, therefore, infer that the circulation structures over the North Atlantic in Figs. 11a and 11c are likely to reflect the favored wave generation under the background flow close to the negative EV2 mode.

On the other hand, the circulation anomalies over the North Atlantic of P1 and P3 do not seem to coincide quite well with the simulated wave response shown in
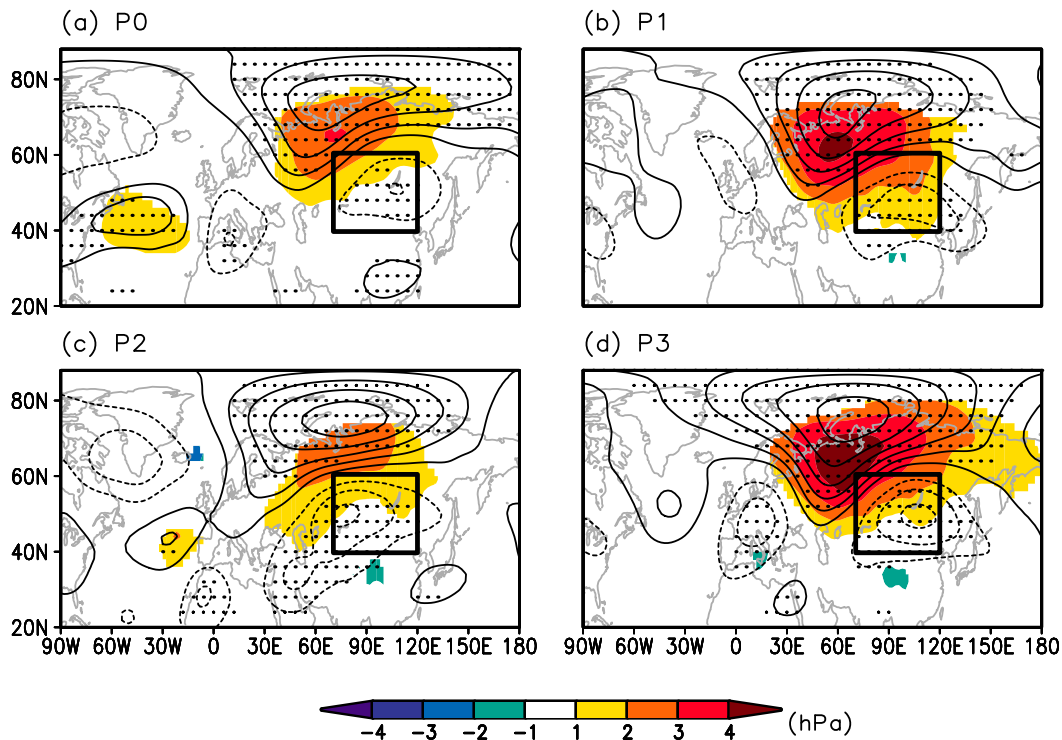
FIG. 11. Linear regression maps of SLP (shading) and Z300 (contours) anomalies onto the WACE index during (a) P0, (b) P1, (c) P2, and (d) P3. The SLP anomalies, which are significant at a 95% confidence level, were shaded only (unit: hPa). Stippled areas indicate a significant deviation of Z300 at 95% confidence level on a t test. Contour intervals are 10 m.

Fig. 10e. But, here we need to pay attention to the coherence between the circulation characteristics of P1 and P3. We further take note of the composite anomalies corresponding to the +WACE pattern in Fig. 4d, which also provide the analogous feature of a weak and insignificant anticyclonic anomaly over the middle of the North Atlantic region. This similarity may allude to the way the forced response is incorporated into the background flow during +EV2 periods in the real atmosphere, although the reason for the weakness of the resultant anomaly over the North Atlantic is not clear. The phase-asymmetric response according to the ±EV2 mode is supposedly due to nonlinearity in the dynamical process to drive the Rossby wave response, which is not examined in detail in this study.

The overall consistent results between the observation and model integration support the reliability of our arguments about the role of interdecadally varying atmospheric background flow over the North Atlantic in the long-term variation of the Eurasian SAT as manifested by the altered WACE pattern. The quasi-stationary Rossby wave favored by the background flow condition of the negative EV2 mode acts to weaken the coupling between the Arctic and Eurasian temperature perturbations. Consequently, it would affect the

second leading EOF in the Eurasian SAT so as to alter the EOF2 during P0 and P2 from that of P1 and P3. Likewise, the Rossby wave that frequently grows under the positive EV2 mode–like background flow would bring about frequent occurrence of the subarctic high and accordingly enhance the WACE pattern through the strong interaction with the SH. This is why the long-term temporal variation of the EV2 mode accords with the correlation between the SH and WACE pattern as shown in Fig. 8.

6. Summary and discussion

Although the sea ice loss and the concurrent warming over the B/K Sea region are widely believed to be responsible for recurrent cold winters over Eurasia, the impact of sea ice loss is still debated (Inoue et al. 2012; Luo et al. 2016; Honda et al. 2009; Kug et al. 2015; McCusker et al. 2016). By examining the internal atmospheric processes that affect the historical change in the WACE pattern, we tried to find insights in the current contrasting arguments. From the analysis of 20CR data since 1901, we identified noteworthy spatiotemporal variability of the WACE pattern at an interdecadal time scale. Specifically, the Eurasian SAT showed a

pronounced meridional contrast between the B/K Sea and central Siberia, which is represented by the WACE pattern during the decades of 1931–55 (P1) and 1981–2013 (P3). By contrast, this tendency became weaker during other decades of 1901–30 (P0) and 1956–80 (P2).

We should be careful to draw any conclusions about interdecadal variations from a statistical analysis of a few more than a hundred years of observation. However, we further found that this interdecadal variability could be largely related to the atmospheric circulation that originates from the North Atlantic. It is suggested that the variation in the climatological wave system over the North Atlantic, represented by so-called EV2 mode, has caused the interdecadal changes in the downstream climate by altering the background flow condition for the quasi-stationary Rossby wave generation. In other words, a deepened (shallow) climatological wave condition over the North Atlantic during P1 and P3 (P0 and P2) [i.e., the +EV2 (−EV2) period] alters the mean atmospheric baroclinicity, storm track intensity, and transient eddy vorticity flux. The resultant changes act as a constraint for the preferable quasi-stationary intraseasonal Rossby wave generation and consequently affect the downstream local circulation characteristics over the B/K Sea region. In detail, the preferred Rossby wave response during each winter of P1 and P3 (P0 and P2) promotes the emergence of the +WACE (−WACE) pattern in the seasonal mean, through the strong (weak) interaction between the anticyclonic (cyclonic) wave branch over the B/K Sea and the SH. These altered atmospheric circulations by decades become manifested as the spatiotemporal variation of the WACE pattern in the interdecadal time scale.

The dynamical process suggested in this study as a cause of the interdecadal variation in the WACE pattern is intimately linked with a recent finding in Jung et al. (2017), who elucidated the warming mechanism over the B/K Sea region focusing on interannual time scale. They concluded that the altered atmospheric baroclinicity over the Gulf Stream region brings about a change in low-frequency wave response that accompanies the warming over the B/K Sea region by exerting a significant warm advection. Their conclusion is based on the characteristic of the oceanic perturbation in the frontal region that can act to sustain the atmospheric baroclinicity, which is alone usually relaxed rapidly through atmospheric heat transport by eddy (Brayshaw et al. 2008; Frankignoul et al. 2011).

The present results further suggest that the impacts of the oceanic perturbation can be also of crucial importance for the interdecadal time scale as well. With regard to this, it is essential to note that the long-term change of the Atlantic meridional overturning circulation (AMOC)

is manifested as a northward warm water flux over the North Atlantic, and the Gulf Stream is tied closely to the strength of the AMOC (de Coëtlogon et al. 2006). These characteristics can possibly imply that the oceanic circulation is involved with the long-term variation of the EV2 mode as well as the WACE pattern, although this study does not address the detailed linkage with the oceanic circulations. Actually, the significant warm and cold anomalies over the North Atlantic front region shown in Figs. 4b and 4c may allude to the involvement of the AMOC in the WACE pattern, and this can be interpreted as implying that the current Arctic warming trend is partially attributable to the internal variability of the Earth climate system to some extent, as argued by Watanabe et al. (2014).

To further support this idea, it is useful to review a study by Kim et al. (2017), who investigated an extreme Arctic warming event that occurred in January 2016. They substantiated the role of a strong Atlantic windstorm that migrated much farther northward toward the Arctic than ordinary storms, and then argued that the windstorm triggered the abrupt warming in the Arctic through warm and moist air intrusion. After the storm terminated at the eastern coast of Greenland, it was followed by a prolonged blocking period that sustained the extreme Arctic warming. Although it was a case study, we infer that these serial processes driving the extreme Arctic warming event may not be completely accidental. We can understand the full context of unusual behavior of the windstorm as well as the abrupt Arctic warming event by tracking the detailed progress manifested in daily weather chart from the perspective of dynamics suggested in the present study. We suppose that the warming event followed by a windstorm and blocking may be incidental to the deepened climatological wave system over the North Atlantic in this decade (see the strong positive magnitude of the long-term averaged EV2 index in Fig. 8). The corresponding southerly wind in the background flow condition may facilitate the storm migration farther northward. During the termination of the windstorm at the eastern coast of Greenland, a vorticity flux would be transferred to a low-frequency wave (Kug and Jin 2009; Jin et al. 2006), and this would affect the growth of the blocking in the Arctic. This temporal evolution of the windstorm shows a dramatic coincidence with what we revealed regarding the intraseasonal circulation characteristics accompanied by the positive EV2 mode (i.e., the anomalous transient eddy vorticity flux convergence over the southeastern coast of Greenland and the subsequent growth of the anticyclonic anomaly over the B/K Sea region). It is quite interesting that much earlier observational studies also had remarked that the largest

positive SAT anomalies appeared during the mid-twentieth century around Svalbard and the northern North Atlantic, associated with an increase in southerly winds and more frequent storms in the region compared to previous decades (Wood and Overland 2010, and references therein). These past changes are highly coherent with the long-term variation of the EV2 mode.

The dynamical processes suggested in this study as controlling the historical change of the WACE pattern clearly show the role of the internal variability inherent in the climate system. According to these results, the current Arctic warming may be a part of oscillatory climate variability. However, we also note that anthropogenic warming processes are so complicated that their impacts are nonlinear and hardly distinguishable from that of the internal variability (Overland et al. 2016). Although we highlighted the Arctic warming over the B/K Sea due to extra-Arctic processes modulated by a long-term internal mode, the response to anthropogenic warming can be also manifested as an amplified intrinsic mode. In this context, we should be cautious about conclusions regarding the impacts of the internal variability. To assess the impacts of the internal variability and anthropogenic change more precisely, it is required to investigate how the EV2 mode responds to remote forcing relevant to other long-term natural variability such as the Pacific decadal variability (England et al. 2014).

This study suggests that we can assess the long-term internal variability of the climatological stationary wave by the EV2 mode, which focuses on the regional meridional wind over the North Atlantic. Interestingly, Teng and Branstator (2012) also had noticed a pronounced long-term variability inherent in the Northern Hemispheric meridional wind. They reported that this long-term variability is largely explained especially by the second EOF of the entire Northern Hemisphere wintertime V300 (20°–90°N), the so-called Wave3 pattern (see their Fig. 3b). We found that the EV2 mode is quite similar to this Wave3 pattern in spatial and temporal variability. Although we addressed the dynamical implication of the long-term variability in the meridional wind in regional perspective only, the resemblance between the EV2 mode and Wave3 pattern suggests further investigation into the dynamical impact of this mode in global perspective. It would be worthwhile for a better understanding of the current climate in the Earth climate system as well as estimating upcoming changes.

REFERENCES

Alexander, M. A., U. S. Bhatt, J. E. Walsh, M. S. Timlin, J. S. Miller, and J. D. Scott, 2004: The atmospheric response to realistic Arctic sea ice anomalies in an AGCM during winter. *J. Climate*, **17**, 890–905, https://doi.org/10.1175/1520-0442(2004)017<0890:TARTRA>2.0.CO;2.

Barnes, E. A., and J. A. Screen, 2015: The impact of Arctic warming on the midlatitude jet-stream: Can it? Has it? Will it? *Wiley Interdiscip. Rev.: Climate Change*, **6**, 277–286, https://doi.org/10.1002/wcc.337.

Bengtsson, L., V. A. Semenov, and O. M. Johannessen, 2004: The early twentieth-century warming in the Arctic—A possible mechanism. *J. Climate*, **17**, 4045–4057, https://doi.org/10.1175/1520-0442(2004)017<4045:TETWIT>2.0.CO;2.

Brayshaw, D. J., B. Hoskins, and M. Blackburn, 2008: The storm-track response to idealized SST perturbations in an aqua-planet GCM. *J. Atmos. Sci.*, **65**, 2842–2860, https://doi.org/10.1175/2008JAS2657.1.

Cohen, J. L., J. C. Furtado, M. A. Barlow, V. A. Alexeev, and J. E. Cherry, 2012: Arctic warming, increasing snow cover and widespread boreal winter cooling. *Environ. Res. Lett.*, **7**, 014007, https://doi.org/10.1088/1748-9326/7/1/014007.

Compo, G. P., and Coauthors, 2011: The Twentieth Century Reanalysis Project. *Quart. J. Roy. Meteor. Soc.*, **137**, 1–28, https://doi.org/10.1002/qj.776.

de Coëtlogon, G., C. Frankignoul, M. Bentsen, C. Delon, H. Haak, S. Masina, and A. Pardaens, 2006: Gulf Stream variability in five oceanic general circulation models. *J. Phys. Oceanogr.*, **36**, 2119–2135, https://doi.org/10.1175/JPO2963.1.

Ding, Y., and T. N. Krishnamurti, 1987: Heat budget of the Siberian high and the winter monsoon. *Mon. Wea. Rev.*, **115**, 2428–2449, https://doi.org/10.1175/1520-0493(1987)115<2428:HBOTSH>2.0.CO;2.

Dole, R., and N. Gordon, 1983: Persistent anomalies of the extratropical Northern Hemisphere wintertime circulation: Geographical distribution and regional persistence characteristics. *Mon. Wea. Rev.*, **111**, 1567–1586, https://doi.org/10.1175/1520-0493(1983)111<1567:PAOTEN>2.0.CO;2.

Dunn-Sigouin, E., S.-W. Son, and H. Lin, 2013: Evaluation of Northern Hemisphere blocking climatology in the Global Environment Multiscale Model. *Mon. Wea. Rev.*, **141**, 707–727, https://doi.org/10.1175/MWR-D-12-00134.1.

England, M. H., and Coauthors, 2014: Recent intensification of wind-driven circulation in the Pacific and the ongoing warming hiatus. *Nat. Climate Change*, **4**, 222–227, https://doi.org/10.1038/nclimate2106.

Frankignoul, C., N. Sennéchael, Y.-H. Kwon, and M. A. Alexander, 2011: Influence of the meridional shifts of the Kuroshio and the Oyashio Extensions on the atmospheric circulation. *J. Climate*, **24**, 762–777, https://doi.org/10.1175/2010JCLI3731.1.

Gong, D.-Y., S. Wang, and J. Zhu, 2001: East Asian winter monsoon and Arctic Oscillation. *Geophys. Res. Lett.*, **28**, 2073–2076, https://doi.org/10.1029/2000GL012311.

Graff, L. S., and J. H. LaCasce, 2012: Changes in the extratropical storm tracks in response to changes in SST in an AGCM. *J. Climate*, **25**, 1854–1870, https://doi.org/10.1175/JCLI-D-11-00174.1.

Graversen, R. G., T. Mauritsen, M. Tjernström, E. Källén, and G. Svensson, 2008: Vertical structure of recent Arctic warming. *Nature*, **541**, 53–56, https://doi.org/10.1038/nature06502.

Hartmann, D. L., 2015: Pacific sea surface temperature and the winter of 2014. *Geophys. Res. Lett.*, **42**, 1894–1902, https://doi.org/10.1002/2015GL063083.

Honda, M., J. Inoue, and S. Yamane, 2009: Influence of low Arctic sea-ice minima on anomalously cold Eurasian winters. *Geophys. Res. Lett.*, **36**, L08707, https://doi.org/10.1029/2008GL037079.

Inoue, J., M. E. Hori, and K. Takaya, 2012: The role of Barents sea ice in the wintertime cyclone track and emergence of a warm-Arctic cold-Siberian anomaly. *J. Climate*, **25**, 2561–2568, https://doi.org/10.1175/JCLI-D-11-00449.1.

Jin, F.-F., L.-L. Pan, and M. Watanabe, 2006: Dynamics of synoptic eddy and low-frequency flow interaction. Part I: A linear closure. *J. Atmos. Sci.*, **63**, 1677–1694, https://doi.org/10.1175/JAS3717.1.

Johannessen, O. M., and Coauthors, 2004: Arctic climate change: Observed and modelled temperature and sea-ice variability. *Tellus*, **56A**, 328–341, https://doi.org/10.3402/tellusa.v56i4.14418.

Joung, C. H., and M. H. Hitchman, 1982: On the role of successive downstream development in East Asian polar air outbreaks. *Mon. Wea. Rev.*, **110**, 1224–1237, https://doi.org/10.1175/1520-0493(1982)110<1224:OTROSD>2.0.CO;2.

Jung, O., M. Sung, K. Sato, Y. Lim, S. Kim, E. Baek, J.-H. Jeong, and B.-M. Kim, 2017: How does the SST variability over the western North Atlantic Ocean control Arctic warming over the Barents–Kara Seas? *Environ. Res. Lett.*, **12**, 034021, https://doi.org/10.1088/1748-9326/aa5f3b.

Kalnay, E., and Coauthors, 1996: The NCEP/NCAR 40-Year Reanalysis Project. *Bull. Amer. Meteor. Soc.*, **77**, 437–471, https://doi.org/10.1175/1520-0477(1996)077<0437:TNYRP>2.0.CO;2.

Karoly, D., and B. Hoskins, 1982: Three-dimensional propagation of planetary waves. *J. Meteor. Soc. Japan*, **60**, 109–123, https://doi.org/10.2151/jmsj1965.60.1_109.

Kim, B.-M., and Coauthors, 2017: Major cause of unprecedented Arctic warming in January 2016: Critical role of an Atlantic windstorm. *Sci. Rep.*, **7**, 40051, https://doi.org/10.1038/srep40051.

Kug, J.-S., and F.-F. Jin, 2009: Left-hand rule for synoptic eddy feedback on low-frequency flow. *Geophys. Res. Lett.*, **36**, L05709, https://doi.org/10.1029/2008GL036435.

——, J.-H. Jeong, Y.-S. Jang, B.-M. Kim, C. K. Folland, S.-K. Min, and S.-W. Son, 2015: Two distinct influences of Arctic warming on cold winters over North America and East Asia. *Nat. Geosci.*, **8**, 759–762, https://doi.org/10.1038/ngeo2517.

Lim, Y.-K., 2015: The East Atlantic/West Russia (EA/WR) teleconnection in the North Atlantic: Climate impact and relation to Rossby wave propagation. *Climate Dyn.*, **44**, 3211–3222, https://doi.org/10.1007/s00382-014-2381-4.

Luo, D., Y. Xiao, Y. Yao, A. Dai, I. Simmonds, and C. L. E. Franzke, 2016: Impact of Ural blocking on winter warm Arctic–cold Eurasian anomalies. Part I: Blocking-induced amplification. *J. Climate*, **29**, 3925–3947, https://doi.org/10.1175/JCLI-D-15-0611.1.

McCusker, K. E., J. C. Fyfe, and M. Sigmond, 2016: Twenty-five winters of unexpected Eurasian cooling unlikely due to Arctic

sea-ice loss. *Nat. Geosci.*, **9**, 838–842, https://doi.org/10.1038/ngeo2820.

Miles, M. W., D. V. Divine, T. Furevik, E. Jansen, M. Moros, and A. E. J. Ogilvie, 2014: A signal of persistent Atlantic multidecadal variability in Arctic sea ice. *Geophys. Res. Lett.*, **41**, 463–469, https://doi.org/10.1002/2013GL058084.

Minobe, S., A. Kuwano-Yoshida, N. Komori, S. Xie, and R. J. Small, 2008: Influence of the Gulf Stream on the troposphere. *Nature*, **452**, 206–209, https://doi.org/10.1038/nature06690.

Mori, M., M. Watanabe, H. Shiogama, J. Inoue, and M. Kimoto, 2014: Robust Arctic sea-ice influence on the frequent Eurasian cold winters in past decades. *Nat. Geosci.*, **7**, 869–874, https://doi.org/10.1038/ngeo2277.

Nakanowatari, T., K. Sato, and J. Inoue, 2014: Predictability of the Barents Sea ice in early winter: Remote effects of oceanic and atmospheric thermal conditions from the North Atlantic. *J. Climate*, **27**, 8884–8901, https://doi.org/10.1175/JCLI-D-14-00125.1.

——, J. Inoue, K. Sato, and T. Kikuchi, 2015: Summertime atmosphere–ocean preconditionings for the Bering Sea ice retreat and the following severe winters in North America. *Environ. Res. Lett.*, **10**, 094023, https://doi.org/10.1088/1748-9326/10/9/094023.

North, G. R., T. L. Bell, R. F. Cahalan, and F. J. Moenig, 1982: Sampling errors in the estimation of empirical orthogonal functions. *Mon. Wea. Rev.*, **110**, 669–706, https://doi.org/10.1175/1520-0493(1982)110<0699:SEITEO>2.0.CO;2.

Ou, T., D. Chen, J.-H. Jeong, H. W. Linderholm, and T. Zhou, 2015: Changes in winter cold surges over southeast China: 1961 to 2012. *Asia-Pac. J. Atmos. Sci.*, **51**, 29–37, https://doi.org/10.1007/s13143-014-0057-y.

Overland, J. E., and Coauthors, 2016: Nonlinear response of midlatitude weather to the changing Arctic. *Nat. Climate Change*, **6**, 992–999, https://doi.org/10.1038/nclimate3121.

Paek, H., and H.-P. Huang, 2012: A comparison of decadal-to-interdecadal variability and trend in reanalysis datasets using atmospheric angular momentum. *J. Climate*, **25**, 4750–4758, https://doi.org/10.1175/JCLI-D-11-00358.1.

Palmer, T., 2014: Record-breaking winters and global climate change. *Science*, **344**, 803–804, https://doi.org/10.1126/science.1255147.

Park, D.-S. R., S. Lee, and S. B. Feldstein, 2015: Attribution of the recent winter sea-ice decline over the Atlantic sector of the Arctic Ocean. *J. Climate*, **28**, 4027–4033, https://doi.org/10.1175/JCLI-D-15-0042.1.

Petoukhov, V., and V. A. Semenov, 2010: A link between reduced Barents-Kara sea ice and cold winter extremes over northern continents. *J. Geophys. Res.*, **115**, D21111, https://doi.org/10.1029/2009JD013568.

Sampe, T., H. Nakamura, A. Goto, and W. Ohfuchi, 2010: Significance of a midlatitude SST frontal zone in the formation of a storm track and an eddy-driven westerly jet. *J. Climate*, **23**, 1793–1814, https://doi.org/10.1175/2009JCLI3163.1.

Sardeshmukh, P. D., and B. J. Hoskins, 1988: The generation of global rotational flow by steady idealized tropical divergence. *J. Atmos. Sci.*, **45**, 1228–1251, https://doi.org/10.1175/1520-0469(1988)045<1228:TGOGRF>2.0.CO;2.

Sato, K., J. Inoue, and M. Watanabe, 2014: Influence of the Gulf Stream on the Barents Sea ice retreat and Eurasian coldness during early winter. *Environ. Res. Lett.*, **9**, 084009, https://doi.org/10.1088/1748-9326/9/8/084009.

Screen, J. A., I. Simmonds, C. Deser, and R. Tomas, 2013: The atmospheric response to three decades of observed Arctic sea

ice loss. *J. Climate*, **26**, 1230–1248, https://doi.org/10.1175/JCLI-D-12-00063.1.

——, C. Deser, I. Simmonds, and R. Tomas, 2014: Atmospheric impacts of Arctic sea-ice loss, 1979–2009: Separating forced change from atmospheric internal variability. *Climate Dyn.*, **43**, 333–344, https://doi.org/10.1007/s00382-013-1830-9.

Sigmond, M., and J. C. Fyfe, 2016: Tropical Pacific impacts on cooling North American winters. *Nat. Climate Change*, **6**, 970–974, https://doi.org/10.1038/nclimate3069.

Sung, M.-K., G.-H. Lim, and J.-S. Kug, 2010: Phase asymmetric downstream development of the North Atlantic Oscillation and its impact on the East Asian winter monsoon. *J. Geophys. Res.*, **115**, D09105, https://doi.org/10.1029/2009JD013153.

——, ——, ——, and S.-I. An, 2011: A linkage between the North Atlantic Oscillation and its downstream development due to the existence of a blocking ridge. *J. Geophys. Res.*, **116**, D11107, https://doi.org/10.1029/2010JD015006.

——, B.-M. Kim, E.-H. Baek, Y.-K. Lim, and S.-J. Kim, 2016: Arctic–North Pacific coupled impacts on the late autumn cold in North America. *Environ. Res. Lett.*, **11**, 084016, https://doi.org/10.1088/1748-9326/11/8/084016.

Takaya, K., and H. Nakamura, 2005a: Mechanisms of intraseasonal amplification of the cold Siberian high. *J. Atmos. Sci.*, **62**, 4423–4440, https://doi.org/10.1175/JAS3629.1.

——, and ——, 2005b: Geographical dependence of upper-level blocking formation associated with intraseasonal amplification of the Siberian high. *J. Atmos. Sci.*, **62**, 4441–4449, https://doi.org/10.1175/JAS3628.1.

Tang, Q., X. Zhang, X. Yang, and J. A. Francis, 2013: Cold winter extremes in northern continents linked to Arctic sea ice loss. *Environ. Res. Lett.*, **8**, 014036, https://doi.org/10.1088/1748-9326/8/1/014036.

Teng, H., and G. Branstator, 2012: A zonal wavenumber 3 pattern of Northern Hemisphere wintertime planetary wave variability at high latitudes. *J. Climate*, **25**, 6756–6769, https://doi.org/10.1175/JCLI-D-11-00664.1.

Thompson, D. W. J., and J. M. Wallace, 1998: The Arctic oscillation signature in the wintertime geopotential height and temperature fields. *Geophys. Res. Lett.*, **25**, 1297–1300, https://doi.org/10.1029/98GL00950.

Tibaldi, S., and F. Molteni, 1990: On the operational predictability of blocking. *Tellus*, **42A**, 343–365, https://doi.org/10.3402/tellusa.v42i3.11882.

Ting, M., and L. Yu, 1998: Steady response to tropical heating in wavy linear and nonlinear baroclinic models. *J. Atmos. Sci.*, **55**, 3565–3582, https://doi.org/10.1175/1520-0469(1998)055<3565:SRTTHI>2.0.CO;2.

Tokinaga, H., S.-P. Xie, and H. Mukougawa, 2017: Early 20th-century Arctic warming intensified by Pacific and Atlantic multidecadal variability. *Proc. Natl. Acad. Sci. USA*, **114**, 6227–6232, https://doi.org/10.1073/pnas.1615880114.

Wang, H., and M. Ting, 1999: Seasonal cycle of the climatological stationary waves in the NCEP–NCAR reanalysis. *J. Atmos. Sci.*, **56**, 3892–3919, https://doi.org/10.1175/1520-0469(1999)056<3892:SCOTCS>2.0.CO;2.

Watanabe, M., H. Shiogama, H. Tatebe, M. Hayashi, M. Ishii, and M. Kimoto, 2014: Contribution of natural decadal variability to global warming acceleration and hiatus. *Nat. Climate Change*, **4**, 893–897, https://doi.org/10.1038/nclimate2355.

Watson, P. A. G., A. Weisheimer, J. R. Knight, and T. N. Palmer, 2016: The role of the tropical West Pacific in the extreme Northern Hemisphere winter of 2013/2014. *J. Geophys. Res. Atmos.*, **121**, 1698–1714, https://doi.org/10.1002/2015JD024048.

Wood, K. R., and J. E. Overland, 2010: Early 20th century Arctic warming in retrospect. *Int. J. Climatol.*, **30**, 1269–1279, https://doi.org/10.1002/joc.1973.

Woods, C., and R. Caballero, 2016: The role of moist intrusions in winter Arctic warming and sea ice decline. *J. Climate*, **29**, 4473–4485, https://doi.org/10.1175/JCLI-D-15-0773.1.

——, ——, and G. Svensson, 2013: Large-scale circulation associated with moisture intrusions into the Arctic during winter. *Geophys. Res. Lett.*, **40**, 4717–4721, https://doi.org/10.1002/grl.50912.

Yang, X.-Y., J. C. Fyfe, and G. M. Flato, 2010: The role of poleward energy transport in Arctic temperature evolution. *Geophys. Res. Lett.*, **37**, L14803, https://doi.org/10.1029/2010GL043934 .

Zhang, X., C. Lu, and Z. Guan, 2012: Weakened cyclones, intensified anticyclones and recent extreme cold winter weather events in Eurasia. *Environ. Res. Lett.*, **7**, 044044, https://doi.org/10.1088/1748-9326/7/4/044044.